NANO LETTERS
Cite This: Nano Lett. 2018, 18, 4482−4486
Letter
pubs.acs.org/NanoLett

The Conductance of Porphyrin-Based Molecular Nanowires Increases with Length

Norah Algethami, Hatef Sadeghi,* Sara Sangtarash, and Colin J. Lambert*

Theory of Molecular Scale Transport, Physics Department, Lancaster University, LA1 4YB Lancaster, United Kingdom

Supporting Information

ABSTRACT: High electrical conductance molecular nanowires are highly desirable components for future molecular-scale circuitry, but typically molecular wires act as tunnel barriers and their conductance decays exponentially with length. Here, we demonstrate that the conductance of fused-oligo-porphyrin nanowires can be either length independent or increase with length at room temperature. We show that this negative attenuation is an intrinsic property of fused-oligo-porphyrin nanowires, but its manifestation depends on the electrode material or anchor groups. This highly desirable, nonclassical behavior signals the quantum nature of transport through such wires. It arises because with increasing length the tendency for electrical conductance to decay is compensated by a decrease in their highest occupied molecular orbital−lowest unoccupied molecular orbital gap. Our study reveals the potential of these molecular wires as interconnects in future molecular-scale circuitry.

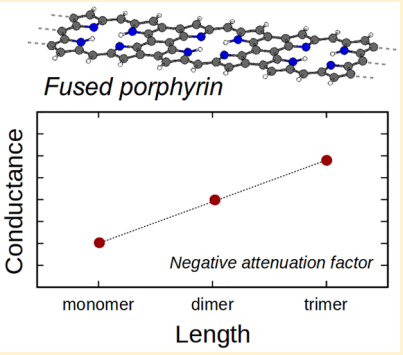

KEYWORDS: *Single molecule electronics, conductance, porphyrin, negative attenuation factor*

The search for molecular nanowires, whose electrical conductance decays slowly with length has been subject to many studies in the last couple of decades.[1−6] Single-molecule wires typically act as tunnel barriers and their conductance G decays exponentially by molecular length[7,8] L as $G = Ae^{-\beta L}$ where A is prefactor and β is the decay (attenuation) factor. Molecular wires usually possess a high beta factor, which limits their potential as interconnects in future molecular-scale circuitry. For example, measured room-temperature values of β range from 2.0−3.4 nm^{-1} for oligo(phenylene-ethynylenes) OPEs,[9] 3.3 nm^{-1} for oligo(aryleneethynylenes) OAEs,[10] 1.7−1.8 nm^{-1} for oligo(phenylene-vinylenes) OPVs,[11] 4.9 nm^{-1} for acenes,[12] 1.7−3.1 nm^{-1} for oligoynes,[11,13] and 8.4 nm^{-1} for alkanes[14] depending on their precise anchor groups to gold electrodes.

The aim of the present paper is to identify molecular wires with vanishing or even a negative value of β, motivated by measurements of molecular wires based on porphyrin derivatives,[15−20] which exhibit exceptionally low attenuation factors, due to their highly conjugated electronic structure. For example, scanning tunneling microscope (STM) measurements using a gold tip and substrate revealed that molecular wires formed from porphyrin units connected to each other through acetylene linkers exhibit a low attenuation factor of β = 0.4 nm^{-1} with both pyridyl and thiol anchors[2,21] and fused-oligo-porphyrin wires with pyridyl anchors[22] exhibited an even lower value of β = 0.2 nm^{-1}. The agreement between these experiments and theories based on phase coherent transport suggests that the electron−phonon interaction[23] is not a dominant effect in porphyrin nanowires up to ∼4 nm.

In what follows, we demonstrate that by employing different anchors, this fascinating family of molecular wires can exhibit vanishing or negative attenuation factors. We demonstrate that a negative attenuation factor is an intrinsic property of the fused-oligo-porphyrins, which arises from the strong coupling between neighboring porphyrin oligomers and a resulting strong decrease in their HOMO−LUMO gap with length. This behavior is in marked contrast the anomalous conductance trends measured in oligothiphenes,[24] which are attributed to extrinsic factors, such as conformational changes of the molecule in the junction,[25] or a peculiarity of iodide anchor groups, which cause short oligomers to lie flat on the substrate electrode.[26]

Here we compute the electrical conductance of the highly conjugated porphyrin wires shown in Figure 1, in which neighboring porphyrins are fused to each other via three single bonds (shown in red in Figure 1). We systematically examined fused-oligo-porphyrin (FOP) wires with different lengths connected to different electrodes with different anchors and consistently found that the conductance of these FOP wires can increase with length and that they possess a negative attenuation factor. This is the first time that negative β-factor wires have been identified and this is significant because these wires are stable and therefore ideal candidates for low-conductance interconnects. To demonstrate that this result is generic and occurs for different electrode materials and anchor groups, we study quantum transport through FOPs (Figure 1a) with three different lengths (Figure 1b−d) sandwiched between either gold electrodes[27,28] with thiol or acetylene anchors. We also study FOPs between graphene electrodes[17,29,30] with either

Received: April 22, 2018
Published: June 7, 2018

DOI: 10.1021/acs.nanolett.8b01621
Nano Lett. 2018, 18, 4482−4486

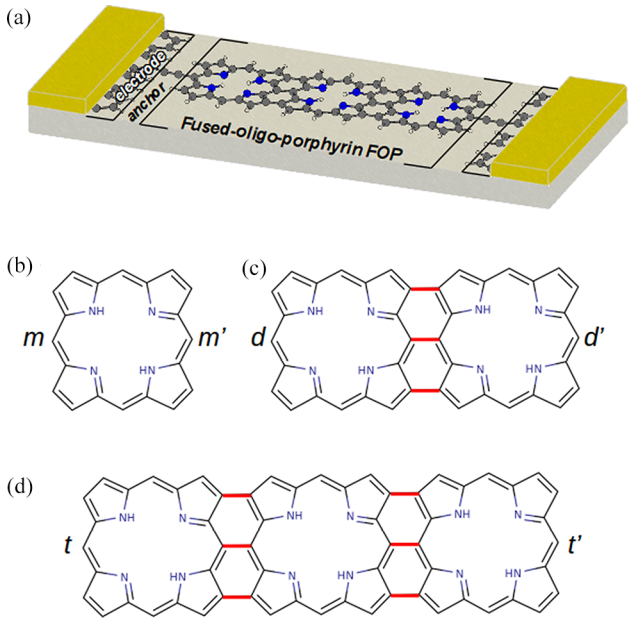

Figure 1. A schematic of a generic molecular junction and FOP monomer, dimer, and trimer molecular wires. (a) The schematic of a generic molecular junction containing a fused porphyrin trimer. (b) A porphyrin monomer connected to electrodes from m and m' connection points. (c) A fused porphyrin dimer, comprising two monomers connected to each other through three single bonds (red bonds) and connected to electrodes from d and d' connection points. (d) A fused porphyrin trimer connected to electrodes from t and t' connection points.

direct carbon−carbon bonds to the edges of the graphene or nonspecific, physisorbed coupling to the graphene.

Figure 1 shows the molecular structure of a porphyrin monomer, a fused dimer, and a fused trimer in which two or three porphyrins are connected to each other through three single bonds (shown by red lines in Figure 1c,d). We first consider molecular junctions in which the carbon atoms labeled (m,m'), (d,d'), and (t,t') are connected to electrodes via acetylene linkers (see SI for the molecular structure of junctions). Figure 2a shows an example of the junction with graphene electrodes (see Figure S1a−c in the SI for the detailed molecular structure) where the porphyrin wires are connected to the edges of rectangular shaped graphene electrodes with periodic boundary conditions in the transverse direction. To calculate the room temperature electrical conductance G, we calculate the electron transmission coefficient $T(E)$ using the Gollum transport code[31] combined with the material specific mean field Hamiltonian obtained from SIESTA implementation of density functional theory (DFT)[32] and then evaluate G using the Landauer formula (see Computational Methods). Results for the monomer, dimer and trimer attached to graphene electrodes (see Figure 2a) are shown in Figure 2b.

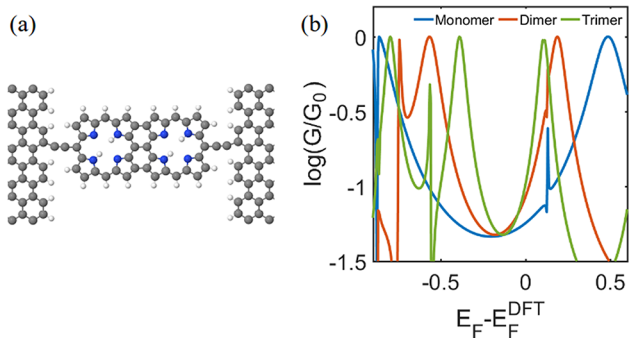

Figure 2. Transport through monomer, dimer, and trimer porphyrin molecular wires attached to two graphene electrodes. (a) A fused porphyrin molecular wire connected to graphene electrodes via acetylene linkers. (b) The room temperature electrical conductance for the porphyrin monomer (blue curve), porphyrin dimer (red curve), and porphyrin trimer (green curve) as a function of the electrode Fermi energy E_F in units of the conductance quantum G_0 = 77 microsiemens.

For these highly conjugated wires, the energy level spacing decreases as their size increases. Therefore, the energy gap between the highest occupied molecular orbital (HOMO) and lowest unoccupied molecular orbital (LUMO) of the dimer is smaller than that of the monomer and in turn, the HOMO−LUMO (HL) gap of the trimer is smaller than that of the dimer. This behavior is reflected in the conductance resonances of Figure 2b, which are furthest apart for the monomer (blue curve) and closest together for the trimer (green curve). This can be understood by starting from a chain of N isolated monomers. Because each monomer has a HOMO energy E_H^0 and a LUMO energy E_L^0, the isolated chain has N-fold degenerate HOMO and N-fold degenerate LUMO. When the monomers are coupled together to form a fused wire, the degeneracies are lifted to yield a HOMO, N-tuplet with molecular orbital energies $E_H^1 < E_H^2 <\cdots< E_H^0 ...< E_H^N$ and a LUMO, N-tuplet $E_L^1 < E_L^2 <\cdots< E_L^0 ...< E_L^N$. Consequently the new HL gap $\Delta(N) = E_L^1 - E_H^N$ is lower in energy than that of the monomer.

Figure 2b shows the electrical conductance as a function of the electrode Fermi energy E_F, plotted relative to the value E_F^{DFT} predicted by DFT for pristine electrodes. The precise value of the electrode Fermi energy E_F can depend on many environmental factors but unless the molecular energy levels are shifted by an electrostatic or electrochemical gate it always lies within the HL gap of the contacted molecule. If $E_F - E_F^{DFT}$ is approximately −0.18 eV, then all three curves in Figure 2b coincide and the monomer, dimer and trimer will possess the same conductance. For any other value within the HL gap (i.e., between the resonant peaks in the range −0.4 to +0.1 eV) the conductance of the trimer exceeds that of the dimer, which in turn exceeds that of the monomer. Consequently, we predict that β is negative or zero.

To demonstrate that negative values of β are a generic feature of FOP molecular wires and occur for different choices of electrode or anchor groups, we calculated their electrical conductances when connected to gold electrodes through thiol anchors (Figure 3a). We also computed their conductances when coupled to graphene electrodes without a conventional anchor group (Figure 3c). For these molecular junctions, Figure 3b,d shows the corresponding electrical conductance. For the gold junctions with thiol anchors, Figure 3b shows that for the thiol-anchored wires, if $E_F - E_F^{DFT}$ is lower than the midgap (0.18 eV) of the trimer, β is zero or slightly positive; otherwise, β is negative.

In the graphene junctions without specific anchoring (Figure 3f), where the overall conductance is low due to the weak physisorbed nature of the coupling to the electrodes, the electrical conductances of FOPs within the HL gap of the trimer are again found to increase with length. This unconventional negative beta factor is clearly independent of the connection point to the electrodes because in the junctions

DOI: 10.1021/acs.nanolett.8b01621
Nano Lett. 2018, 18, 4482−4486

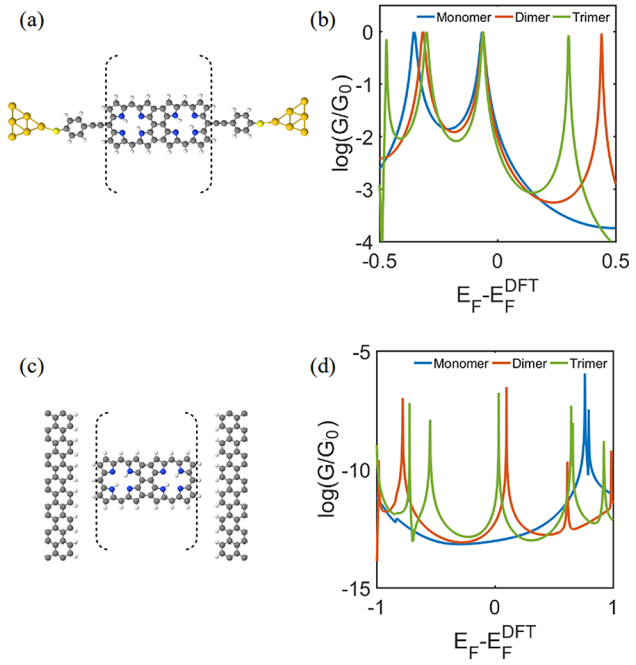

Figure 3. Transport through fused monomer, dimer, and trimer porphyrin wires sandwiched between two graphene or gold electrodes (see Figures S2 and S3 in the SI for molecular structure of all junctions). (a) A gold/dimer/gold junction with thiol anchors. (b) The electrical conductances of the gold/monomer, dimer, or trimer/gold junctions with thiol anchors. The distance between the molecules with gold electrodes and carbon (sulfur) atom is 0.214 nm (0.26 nm). (c) Graphene/monomer, dimer, or trimer/graphene junctions without specific anchoring to the graphene. The distance between FOP and graphene electrodes are 0.3 nm. (d) The electrical conductances graphene/monomer, dimer, or trimer/graphene junctions without specific anchoring to the graphene.

of Figure 3c (see Figure S3 in the SI for details of structure) there is no specific connection point between the electrode surfaces and the molecules. The results of Figures 2 and 3 demonstrate that low or negative β-factors are a common feature of fused oligoporphyrins and occur for different modes of anchoring to electrodes.

To clarify why the conductance increases with length, we constructed a simple tight-binding model in which a single p orbital per atom interacts with nearest neighbor orbitals only. The energy origin is chosen such that all on-site energies are zero except for nitrogens (see Computational Methods) and the energy scale is chosen such that all intraporphyrin nearest-neighbor couplings are set to $\gamma = -1$. We calculated the transmission function $T(E)$ between two ends of the wires, for example, (with contact atoms (m,m'), (d,d'), and (t,t') for the monomer, dimer, and trimer respectively, as shown in Figure 1). We then examined the effect of varying the coupling parameter α between neighboring porphyrin units (shown by red bonds in Figure 1c,d). The different curves in Figure 4a show that for a value $\alpha = 0.65\gamma$ where γ=-1 is coupling integrals between p orbitals of any neighboring C−C atoms,, the curves overlap and for more negative values of α, the transmission coefficient increases with length for energies within the HL gap of the trimer (Figure 4a), in agreement to the above DFT results. To demonstrate that the decrease in the HL gap is due to a splitting of the HOMO and LUMO degeneracies, Figure 4b shows the transmission curves of the trimer over a larger range of energy, for a series of values of the coupling α. For small α, the HOMO and LUMO are each almost triply degenerate and as the magnitude of α increases, the degeneracy is increasingly lifted, leading to a reduction in the HL gap.

For $\alpha = 0.65\gamma$, Figure S7 of the SI shows that this increase in conductance with length persists even if the number of fused porphyrin units increased to 4, 5, and 6 units. On the other hand, Figure 4c shows that the band structure of an infinitely periodic fused porphyrin wire, calculated using density functional theory, possesses a small energy gap of about ∼100 meV. Therefore, fused porphyrin ribbons are narrow-gap semiconductors, meaning that eventually the conductance will begin to decrease with length. In practice, this decrease is likely to be slower than exponential, because at room temperature and large enough length scales, inelastic scattering will become significant and a crossover from phase-coherent tunnelling to incoherent hopping will occur.[10,33] For comparison, Figure S5 of the SI shows the transmission curves for butadiyne-linked porphyrin monomer, dimer, and trimer molecular wires for which the attenuation factor β is clearly positive for a wide range of energies within the HL gap of the trimer in agreement with the reported measured values.[21] The fact that fused porphyrin ribbons are narrow-gap semiconductors means that for a finite oligomer, when electrons tunnel through the gap there will be contributions to the transmission coefficient from both the HOMO and the LUMO bands. Figure S9 of the SI shows that the qualitative features of Figure 4a and Figure 2 can be obtained by summing these two contributions.

The tight-binding results of Figure 4a and the DFT results with a nonspecific anchor (Figure 3d) suggest that a negative

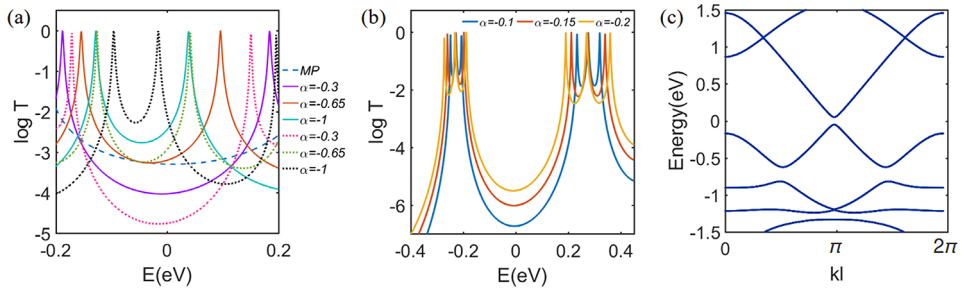

Figure 4. Transmission coefficient for three connections point (m,m'), (d,d'), and (t,t') shown in Figure 1b−d, respectively, obtained using a simple tight binding TB model of FOP junctions. (a) The dash line curve shows the transmission coefficients for the monomer. The solid and dotted lines show the transmission coefficient for the dimer and trimer, respectively. The solid red and dotted green curves show the transmission coefficient for the dimer and trimer when $\alpha = -0.65$. (b) The transmission coefficient of the trimer for values of $\alpha = -0.1, -0.15, -0.2$. (c) Band structure of fused porphyrin nanoribbon.

DOI: 10.1021/acs.nanolett.8b01621
Nano Lett. 2018, 18, 4482−4486

beta factor is a generic feature of the fused porphyrin core, provided the centers of the HOMO−LUMO gaps of the monomer, dimer and trimer are coincident. However, whether or not it is measured experimentally depends on level shifts of molecular orbitals after attaching to the electrodes. This is illustrated by the calculations shown in Figure S10 in the SI using direct C−Au covalent anchoring to gold electrodes, where the HOMOs of the monomer, dimer, and trimer coincide and therefore the centers of their HOMO−LUMO gaps are not coincident. This spoils the generic trend and leads to a positive beta factor. It is worth to mention that the magnitude of the electrical conductance is generally higher in the junctions formed by covalent bond to the graphene electrodes (Figure 2b) compared to junctions formed by gold electrodes (Figures 3b and S10). However, the predicted conductance for the gold junctions with the thiol and direct Au−C anchoring are similar. Depending on the choice of Fermi energy, one might be higher than another as shown in Figure S11.

In summary, we have demonstrated that the electrical conductance of fused oligoporphyrin molecular wires can either increase with increasing length or be length independent in junctions formed with graphene electrodes. This is due to alignment of the middle of the HOMO−LUMO gap of the molecules with the Fermi energy of the graphene electrodes. In addition, we show that in junctions formed with gold electrodes this generic feature is anchor group dependent. This negative attenuation factor is due to the quantum nature of electron transport through such wires and arises from the narrowing of the HOMO−LUMO gap as the length of the oligomers increases.

Computational Methods. The Hamiltonian of the structures described in this paper was obtained using DFT (as described below) or constructed from a simple tight-binding approximation with a single orbital per atom of site energy $\varepsilon = 0$ and $-0.5/\gamma$ for carbon and nitrogen, respectively, and nearest-neighbor couplings $\gamma = -1$ for both C—C and C—N bonds. Single bonds connecting different FOP units in Figure 1 (red bond) is $\alpha = 0.65\gamma$.

DFT Calculation. The geometry of each structure consisting of electrodes (either graphene or gold) and aromatic porphyrin molecule was relaxed to a force tolerance of 20 meV/Å using the SIESTA[32] implementation of DFT with a double-ζ polarized basis set (DZP) and generalized gradient functional approximation (GGA-PBE) for the exchange and correlation functional. A real space grid was defined with an equivalent energy cutoff 150 Ry. The k-point grid of $1 \times 1 \times 20$ was chosen for band structure calculation.

Transport Calculation. The mean-field Hamiltonian obtained from the converged DFT calculation or a simple tight-binding Hamiltonian was combined with our implementation of the nonequilibrium Green's function method, Gollum,[31] to calculate the phase-coherent, elastic scattering properties of each system consist of left (source) and right (drain) leads and the scattering region (molecule). The transmission coefficient $T(E)$ for electrons of energy E (passing from the source to the drain) is calculated via the Landauer formula $G = G_0 \int_{-\infty}^{+\infty} dE T(E)\left(-\frac{\partial f(E)}{\partial E}\right)$ where $f(E)$ is the Fermi distribution function, $G_0 = \frac{2e^2}{h}$ is the conductance quantum, e is the electron charge, and h is Planck's constant.

■ ASSOCIATED CONTENT

Supporting Information

The Supporting Information is available free of charge on the ACS Publications website at DOI: 10.1021/acs.nanolett.8b01621.

Details of geometries, molecular orbital iso-surfaces, simple tight-binding model, and additional transport calculation of molecular junctions with longer length (PDF)

■ AUTHOR INFORMATION

Corresponding Authors

*E-mail: h.sadeghi@lancaster.ac.uk.
*E-mail: c.lambert@lancaster.ac.uk.

ORCID

Hatef Sadeghi: 0000-0001-5398-8620
Colin J. Lambert: 0000-0003-2332-9610

Notes

The authors declare no competing financial interest.

■ ACKNOWLEDGMENTS

H.S. acknowledges the Leverhulme Trust for Leverhulme Early Career Fellowship no. ECF-2017-186. Further support from the UK EPSRC is acknowledged through Grants EP/M014452/1, EP/P027156/1, EP/N017188/1, and EP/N03337X/1.

■ REFERENCES

(1) Sadeghi, H.; Sangtarash, S.; Lambert, C. *Nano Lett.* **2017**, *17* (8), 4611−4618.
(2) Sedghi, G.; Sawada, K.; Esdaile, L. J.; Hoffmann, M.; Anderson, H. L.; Bethell, D.; Haiss, W.; Higgins, S. J.; Nichols, R. J. *J. Am. Chem. Soc.* **2008**, *130* (27), 8582−8583.
(3) Fan, F. R. F.; Yang, J.; Cai, L.; Price, D. W.; Dirk, S. M.; Kosynkin, D. V.; Yao, Y.; Rawlett, A. M.; Tour, J. M.; Bard, A. J. *J. Am. Chem. Soc.* **2002**, *124* (19), 5550−5560.
(4) Bergren, A. J.; McCreery, R. L.; Stoyanov, S. R.; Gusarov, S.; Kovalenko, A. *J. Phys. Chem. C* **2010**, *114* (37), 15806−15815.
(5) Ferreira, Q.; Bragança, A. M.; Alcácer, L.; Morgado, J. *J. Phys. Chem. C* **2014**, *118* (13), 7229−7234.
(6) Ashwell, G. J.; Urasinska, B.; Wang, C.; Bryce, M. R.; Grace, I.; Lambert, C. J. *Chem. Commun.* **2006**, *45*, 4706.
(7) Sadeghi, H. arXiv:1607.02484, 2016. https://arxiv.org/abs/1607.02484.
(8) Sangtarash, S.; Vezzoli, A.; Sadeghi, H.; Ferri, N.; Brien, H. M. O.; et al. *Nanoscale* **2018**, *10*, 3060−3067.
(9) Kaliginedi, V.; Moreno-García, P.; Valkenier, H.; Hong, W.; García-Suárez, V. M.; Buiter, P.; Otten, J. L. H.; Hummelen, J. C.; Lambert, C. J.; Wandlowski, T. *J. Am. Chem. Soc.* **2012**, *134* (11), 5262−5275.
(10) Zhao, X.; Huang, C.; Gulcur, M.; Batsanov, A. S.; Baghernejad, M.; Hong, W.; Bryce, M. R.; Wandlowski, T. *Chem. Mater.* **2013**, *25* (21), 4340−4347.
(11) Moreno-García, P.; Gulcur, M.; Manrique, D. Z.; Pope, T.; Hong, W.; Kaliginedi, V.; Huang, C.; Batsanov, A. S.; Bryce, M. R.; Lambert, C.; Wandlowski, T. *J. Am. Chem. Soc.* **2013**, *135* (33), 12228−12240.
(12) Kim, B.; Beebe, J. M.; Jun, Y.; Zhu, X. Y.; Frisbie, G. D. *J. Am. Chem. Soc.* **2006**, *128* (15), 4970−4971.
(13) Sadeghi, H.; Sangtarash, S.; Lambert, C. J. *Nano Lett.* **2015**, *15* (11), 7467−7472.
(14) Liu, H.; Wang, N.; Zhao, J.; Guo, Y.; Yin, X.; Boey, F. Y. C.; Zhang, H. *ChemPhysChem* **2008**, *9* (10), 1416−1424.

DOI: 10.1021/acs.nanolett.8b01621
Nano Lett. 2018, 18, 4482−4486

(15) Li, Z.; Park, T. H.; Rawson, J.; Therien, M. J.; Borguet, E. *Nano Lett.* **2012**, *12* (6), 2722−2727.
(16) Li, Z.; Borguet, E. *J. Am. Chem. Soc.* **2012**, *134* (1), 63−66.
(17) Mol, J. A.; Lau, C. S.; Lewis, W. J. M.; Sadeghi, H.; Roche, C.; Cnossen, A.; Warner, J. H.; Lambert, C. J.; Anderson, H. L.; Briggs, G. A. D. *Nanoscale* **2015**, *7* (31), 13181−13185.
(18) Winters, M. U.; Dahlstedt, E.; Blades, H. E.; Wilson, C. J.; Frampton, M. J.; Anderson, H. L.; Albinsson, B. *J. Am. Chem. Soc.* **2007**, *129* (14), 4291−4297.
(19) Grozema, F. C.; Houarner-Rassin, C.; Prins, P.; Siebbeles, L. D. A.; Anderson, H. L. *J. Am. Chem. Soc.* **2007**, *129* (44), 13370−13371.
(20) Li, Z.; Smeu, M.; Ratner, M. A.; Borguet, E. *J. Phys. Chem. C* **2013**, *117* (29), 14890−14898.
(21) Sedghi, G.; García-Suárez, V. M.; Esdaile, L. J.; Anderson, H. L.; Lambert, C. J.; Martín, S.; Bethell, D.; Higgins, S. J.; Elliott, M.; Bennett, N.; MacDonald, J. E.; Nichols, R. J. *Nat. Nanotechnol.* **2011**, *6* (8), 517−523.
(22) Sedghi, G.; Esdaile, L. J.; Anderson, H. L.; Martin, S.; Bethell, D.; Higgins, S. J.; Nichols, R. J. *Adv. Mater.* **2012**, *24* (5), 653−657.
(23) Nitzan, A. *Annu. Rev. Phys. Chem.* **2001**, *52* (1), 681−750.
(24) Xu, B. Q.; Li, X. L.; Xiao, X. Y.; Sakaguchi, H.; Tao, N. J. *Nano Lett.* **2005**, *5* (7), 1491−1495.
(25) Capozzi, B.; Dell, E. J.; Berkelbach, T. C.; Reichman, D. R.; Venkataraman, L.; Campos, L. M. *J. Am. Chem. Soc.* **2014**, *136* (29), 10486−10492.
(26) Xiang, L.; Hines, T.; Palma, J. L.; Lu, X.; Mujica, V.; Ratner, M. A.; Zhou, G.; Tao, N. *J. Am. Chem. Soc.* **2016**, *138* (2), 679−687.
(27) Perrin, M. L.; Verzijl, C. J. O.; Martin, C. A.; Shaikh, A. J.; Eelkema, R.; Van Esch, J. H.; Van Ruitenbeek, J. M.; Thijssen, J. M.; Van Der Zant, H. S. J.; Dulić, D. *Nat. Nanotechnol.* **2013**, *8* (4), 282−287.
(28) Perrin, M. L.; Martin, C. A.; Prins, F.; Shaikh, A. J.; Eelkema, R.; van Esch, J. H.; van Ruitenbeek, J. M.; van der Zant, H. S. J.; Dulić, D. *Beilstein J. Nanotechnol.* **2011**, *2* (1), 714−719.
(29) Sadeghi, H.; Mol, J.; Lau, C.; Briggs, A.; Warner, J.; Lambert, C. J. *Proc. Natl. Acad. Sci. U. S. A.* **2015**, *112* (9), 2658−2663.
(30) Sadeghi, H.; Sangtarash, S.; Lambert, C. J. *Beilstein J. Nanotechnol.* **2015**, *6* (1), 1413−1420.
(31) Ferrer, J.; Lambert, C. J.; García-Suárez, V. M.; Manrique, D. Z.; Visontai, D.; Oroszlany, L.; Rodríguez-Ferradás, R.; Grace, I.; Bailey, S. W. D.; Gillemot, K.; Sadeghi, H.; Algharagholy, L. A. *New J. Phys.* **2014**, *16*, 093029.
(32) Soler, J. M. J. M.; Artacho, E.; Gale, J. D.; García, A.; Junquera, J.; Ordejón, P.; Sánchez-Portal, D.; Garcìa, A.; Junquera, J.; Ordejòn, P.; Sànchez-Portal, D.; Garcia, A.; Junquera, J.; Ordejon, P.; Sanchez-Portal, D. *J. Phys.: Condens. Matter* **2002**, *14* (11), 2745−2779.
(33) Choi, S. H.; Kim, B.; Frisbie, C. D. *Science* **2008**, *320* (5882), 1482−1486.

DOI: 10.1021/acs.nanolett.8b01621
Nano Lett. 2018, 18, 4482−4486